Cathode heating mechanisms in pseudospark plasma switches

Timothy J. Sommerer,[a] Hoyoung Pak,[b] and Mark J. Kushner[c]
Department of Electrical and Computer Engineering, University of Illinois, 1406 West Green Street, Urbana, Illinois 61801

(Received 17 April 1992; accepted for publication 18 June 1992)

Pseudosparks, and the back-lighted thyratron (BLT) in particular, are finding increasing application as pulse power switches. An attractive feature of BLTs is that high current densities ($>$ tens of kA cm^{-2}) can be sustained from metal cathodes without auxiliary heating. The source of this current is believed to be electric-field-enhanced thermionic emission resulting from heating of the cathode by ion bombardment during commutation which ultimately melts the surface of the cathode. It is proposed that a photon-driven ionization mechanism in the interelectrode gap of the BLT is responsible for initiating the observed patterns of cathode surface melting and electron emission. A $2\frac{1}{2}$-dimensional computer model is presented that incorporates a photo-induced ionization mechanism to spread the plasma into the interelectrode gap. It predicts a melting of the cathode in a pattern similar to that which is experimentally observed, and predicts a rate of field-enhanced thermionic electron emission that is sufficient to explain the high BLT conduction current density. In the absence of these mechanisms, the model does not predict the observed large-area melting of the face of the cathode. The cathode heating rate during the BLT switching phase is maximum for operating parameters that are very close to the limit for which the switch will close (that is, the smallest possible pressure-electrode spacing product and smallest possible electrode holes).

I. INTRODUCTION

Pseudosparks are low-pressure plasma devices (<1 Torr) now being developed as high-voltage switches.[1–5] As low-pressure switches, pseudospark switches are best described as thyratrons, which obtain holdoff by operating at low values of pressure $\times$ electrode spacing (*pd* product). In spite of operating at low pressures (<1 Torr), pseudosparks have demonstrated the current carrying capability of high-pressure switches (>1 atm) such as spark gaps. Holdoff voltages of >72 kV and currents of >80 kA have recently been achieved in a single-gap device.[6]

Back-lighted thyratrons (BLTs) are a variant of pseudosparks.[1,3,6] These devices differ from conventional pseudosparks by being triggered by photoelectron emission resulting by ultraviolet (UV) illumination of the cathode. A schematic of a typical BLT is shown in Fig. 1. The cathode and anode consist of opposing hollow structures with a central hole. Externally generated UV photons are directed through a window onto the inner surface of the cathode, producing photoelectrons. The photoelectrons convect under the influence of the vacuum fields and cause ionization in the central hole and gap. This ionization leads to an electric-field configuration inside the cathode resembling a hollow cathode, which is believed to be required for triggering.

The commutation and conduction phases of BLT operation are distinctly different. During commutation, the BLT appears to operate as a conventional glow discharge with current from the cathode being sustained primarily by secondary electron emission.[7,8] At this stage, the majority of current appears to pass through the cathode and anode holes after having been generated by ion impact on the interior surfaces of the cathode. Toward the end of commutation and at the onset of conduction, the source of current quickly changes to the opposing faces of the cathode and anode (location A in Fig. 1). The current densities at these locations increase to tens of kA cm^{-2}. Inspection of the cathode surfaces provides clear evidence that there is melting in an annular region surrounding the central hole in spite of there being no auxiliary heating. The transition to thermionic emission occurs on a tens of ns timescale.

Given these observations, Hartmann *et al.*[1,2] have proposed that the source of current is electric-field-enhanced thermionic emission. In this mechanism, the face of the cathode is heated by ion bombardment during commutation while the voltage is still high. As plasma begins to form in the gap, a sheath of only a few to tens of μm thick forms at the cathode surface. This leads to a commensurately large electric field at the surface of the cathode which, coupled with the cathode heating, is the source of the electron emission. Other explanations have been proposed which suggest that when the plasma density in the gap gets sufficiently large, and sheath thickness sufficiently small, the cathode surface may emit in a manner similar to a vacuum arc. In either case, there must be a fairly high plasma density (10^{12}–10^{13} cm^{-3}) in the gap before the sheath is small enough for these electric-field-enhanced processes to occur.

The details of thermionically enhanced electric-field emission have been discussed in detail in the context of sustaining current in the BLT and computer models of plasma dynamics in the BLT have been published describ-

[a]Present address: General Electric, Inc., Research and Development, P.O. Box 8, Schenectady, NY 12301.
[b]Present address: Sandia National Laboratory, Albuquerque, NM 87185.
[c]Author to whom correspondence should be addressed.

 0021-8979/92/203374-10$04.00

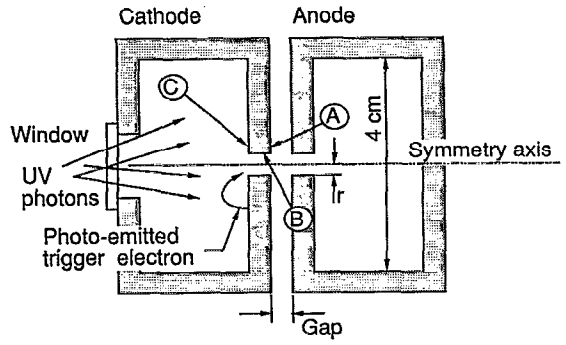

FIG. 1. A schematic of the BLT that consists of opposing hollow cylindrical electrodes with central holes. UV photons entering through the window generate photoelectrons from the back side of the cathode, which then avalanche as they are swept through the cathode hole. Locations A, B, and C are the face of the cathode, surface of the cathode hole, and surface of the hollow cathode, respectively.

ing the operation of the BLT.[7–11] The pertinent experimental observation that current comes from and melting occurs on the face of the cathode has yet to be explained. The missing component is the manner in which ions transport from the axis to the inner portion of the gap or generated in the gap to provide the necessary ion bombardment, or how plasma is formed within the gap to shrink the sheath so that electric-field-enhanced processes can take over.

In this paper, we present a possible explanation for the onset of thermionic emission in pseudosparks based on the results of hydrodynamic computer model for the BLT. The model includes the pertinent electron and ion transport equations, and detailed descriptions of cathode heating and sheath dynamics. An added feature of the model is the inclusion of transport of ionizing radiation from the axis to the gap as the source of seed ions for heating. In the following sections, we describe our models for the BLT, discuss the various mechanisms which may be responsible for generating seed ions in the gap, and finally present results from our model which support the photoionization mechanism.

II. DESCRIPTION OF THE BEAM-BULK MODEL

We previously presented a model applicable to the triggering and switching phases of BLT operation.[7,9,10] That work serves as a basis for the model whose results we present here. The previous model will be briefly described followed by a discussion of the enhancements we have implemented to study cathode heating.

The basic model is a $2\frac{1}{2}$-dimensional plasma fluid model. An electron fluid and a singly charged H_2-ion fluid are integrated forward in time along with Poisson's equation for the electric field to self-consistently simulate the time evolution of the plasma during commutation in a BLT. Ions are always considered to be in equilibrium with the local electric field in the bulk plasma, and their drift velocity and diffusion coefficients are therefore given by the local electric field. Electrons are less likely to be in equilibrium with the local electric field, so additional conservation equations for momentum and energy can be included. Additionally, electron "beams" can be used in the model to describe the highly energetic runaway electrons which can form in the high E/N (electric field/neutral gas density) found in a typical BLT.

The individual mechanisms in the electron model can be arbitrarily included or excluded to test their importance. At its simplest, the electron fluid is modeled as being in equilibrium with the local electric field (a drift-diffusion model). The most sophisticated possibility includes the continuity, momentum, and energy equations for the electron fluid, and additionally models directed electrons as monoenergetic "beams." In previous work, for example, we found that the predicted current rise $I(t)$ (and hence the switching time) was well characterized by the simple drift-diffusion electron model. It was necessary, however, to consider the electron momentum and energy equations in order for the model to faithfully predict the formation of an experimentally observed intense electron beam.[5]

III. DESCRIPTION OF THE CATHODE HEATING MODEL

The goal of the present work is to extend the just-described model to study BLT cathode heating and electron emission. In this section, we will detail three significant additions to the previous model: an accurate description of the BLT during the high-density conduction phase, the addition of a realistic external circuit, and a model of the cathode heating and emission. Even with these processes included, however, the observed cathode melting and superdense glow cannot be explained. Additional physical mechanisms will be considered in Sec. IV.

A. Modifications to the plasma model

Gas-phase dissociation and ionization of the feedstock H_2 gas can occur during the conduction phase. Gas-phase depletion is estimated to peak at 1%–10% of the feedstock density during commutation. The density of feedstock H_2 is calculated during the simulation by incorporating the appropriate rate equations to account for depletion by ionization while presuming negligible diffusion of the H_2 during the time of interest (tens to hundreds of ns).

Due to the high plasma density, the integration time step Δt is dynamically determined and set to be $0.1\tau_{DR} < \Delta t < \tau_{DR}$, where τ_{DR} is the dielectric relaxation time.[12] Though an implicit time-integration scheme is desirable and has been used to model BLT operation,[8] the time integration here is explicit. We have, however, reduced the computational load by making the integration only first-order accurate. (The models presented in Refs. 9 and 10 are fourth-order accurate.) For all but the initial transient ($I \ll 1$ A), the dielectric relaxation time is typically much smaller than that required to satisfy the Courant limit for electron fluid flow, so the first-order integration is both stable and accurate.

Several mechanisms that are not important prior to conduction, but which may become important during or after conduction, have also been neglected. Dissociation of H_2 into neutral atomic H may be significant. Such dissoci-

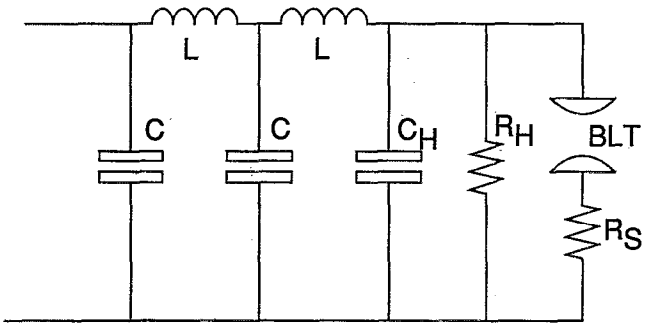

FIG. 2. Schematic of the external pulse forming line (PFL) circuit we used in our model.

ation might increase the ambient pressure by a factor of ≈ 2 and may therefore enhance electron multiplication. Similarly, gas-phase shockwaves and beam instabilities have been considered as sources of enhanced gas-phase ionization.[3] These mechanisms can be difficult to quantify, both because the BLT operating environment is far from ideal, and because the fluid plasma model does not contain sufficient physics to accurately represent shocks.

B. The external circuit

The triggering and switching phases of BLT operation can be modeled to first order by presuming that the voltage across the BLT is fixed. The model presented in Ref. 9 presumed a constant voltage source with an external load resistor in series with the BLT to simulate the initial phases of the voltage collapse during switching. A proper model of the commutation phase requires that we consider the finite energy available in stray capacitances that are close coupled to the BLT.

We have modeled the external pulse-forming line (PFL) with the circuit shown in Fig. 2. The values of the elements of the circuit are uniquely specified by the impedance Z_{PFL} and two-way transit time t_{PFL} of the PFL. The BLT switch element consists of a resistive component R_{BLT} which is determined by the plasma model, a load resistor R_S, a head resistance R_H, and head capacitance C_H. Appropriate rate equations are included in the model to describe the various currents and voltages in the circuit. We included ten stages in the PFL with element values of $C_H = 10$ pF, $R_H = 10^7\ \Omega$, and $R_S = 1\ \Omega$. C and L were chosen so that the PFL impedance $Z = 2.5\ \Omega$ and we had a transit time of 6.7 ns.

C. Field-enhanced thermionic emission model

Hartmann *et al.*[1,2] have reviewed the heating of metal surfaces for typical BLT conditions. The surface temperature at location s and depth x can be found knowing the history of the power deposition on the surface $P(s,t)$,

$$T(s,t,x)-T_0=\frac{\kappa^{1/2}}{K\pi^{1/2}}\int_0^t \frac{dt'}{t'^{1/2}}P(s,t-t')\exp\left(\frac{-x^2}{4\kappa t'}\right). \quad (1)$$

TABLE I. Field-enhanced thermionic emission parameters for molybdenum cathode surface (see Refs. 13–15).

Symbol	Value	Description
c_s	0.059 cal g^{-1} K^{-1}	Specific heat
ρ_m	10.22 g cm^{-3}	Mass density
K	1.38 W cm^{-1} K^{-1}	Thermal conductivity
T_m	2895 K	Melting point
A	55 A K^{-2} cm^{-2}	Thermionic emission coefficient
ϕ	4.3 eV	Work function

Here T_0 is the initial temperature, $\kappa = K/(\rho c_s)$, where c_s and ρ_m are the heat capacity and mass density, respectively, of the cathode surface. K is the thermal conductivity and P is the heating power flux, which is described below. We have chosen values for these parameters which correspond to a Mo cathode surface (Table I). The location variable s corresponds to a position along the cathode surface: hence, each s corresponds to a unique (r,z) coordinate. The power density at the surface is the sum of energetic ion impact and electron-ion recombination on the surface. Once the surface temperature and electric field are known, the electron emission can be found from the Fowler–Nordheim–Bethe–Sommerfeld (FNBS) equation,[16]

$$j_{\mathrm{FNBS}}=AT^2\int_{-\infty}^{\infty}\ln\left[1+\exp\left(\frac{-eV}{kT}\right)\right]T(V)d\left(\frac{eV}{kT}\right). \quad (2)$$

Here A is the thermionic emission coefficient, and $T(V)$ is a factor that takes into account the change in the work function of the surface at high-electric-field values. $T(V)$ is determined from the following equations (in mks units):

$$T(V)=1, \qquad \phi-\delta\phi<V<\infty, \quad (3a)$$

$$=\exp[-6.83\times10^7\times(\phi-V)^{3/2}f(y)/E], \qquad -\infty<V<\phi-\delta\phi, \quad (3b)$$

$$y=\frac{\delta\phi}{\phi-V}, \quad \delta\phi=3.79\times10^{-4}E^{1/2}. \quad (3c)$$

The surface electric-field strength is E, ϕ is the cathode surface work function at zero electric field, and $f(y)$ is an eliptic function that accounts for the image force, and is tabulated in Ref. 16. The effect that results from including the electric-field enhancement of the thermionic emission is a rapid turn on of emission at moderate temperatures. These equations are implemented by loading the results of the numerical integral into an array and then interpolating the array during execution of the model for thermal emission current as a function of temperature and field.

Given an arbitrarily fine computational mesh, the power flux and electric-field strength at the surface can be directly obtained from the BLT model from the solution of Poisson's equation and the ion continuity equations. The sheaths of the cathode fall, however, become exceedingly narrow during the BLT conduction phase (a few μm), and an unreasonable number of mesh points would be required

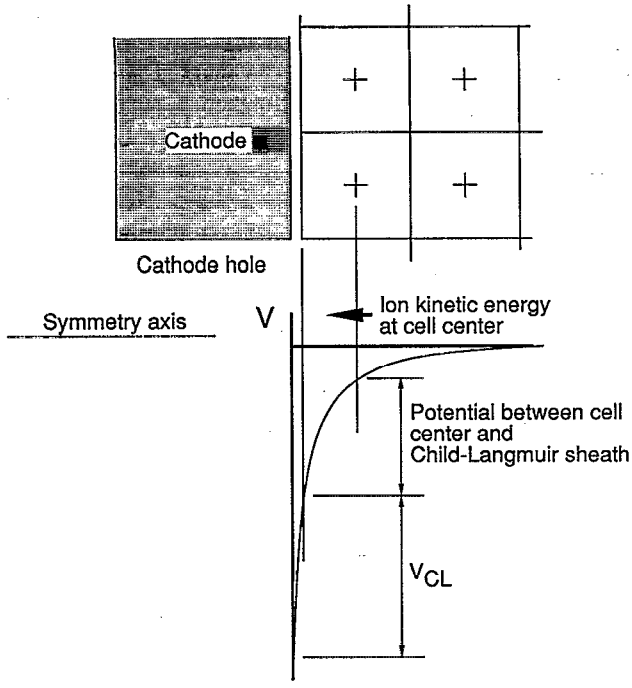

FIG. 3. Relationship between the cathode face, the Child–Langmuir (CL) sheath, and the numerical mesh on which the model calculates electric potentials. When the thickness of the cathode sheath decreases below the width of a numerical cell, the numerical mesh is displaced from the surface of the cathode by the thickness of the CL sheath. The boundary condition for solving Poisson's equation on the numerical mesh is then $V(\text{cathode})+V_{CL}$. The ion energy striking the cathode is the sum of the ion kinetic energy at the center of the boundary cell and the potential energy measured to the cathode surface.

to resolve the near-cathode region on this spatial scale. This situation is remedied in the following fashion.

During the initial phases of BLT operation, the electric potential is calculated on a mesh which is presumed to be in contact with the cathode surface. The voltage at the last mesh point is then the same as the cathode potential. As the ion current increases, however, the cathode sheath contracts. When it is ≈ 1 spatial cell wide the sheath can no longer be resolved and the calculated sheath becomes "mesh limited" while the real sheath continues to contract. To further resolve the sheath under these conditions, we assumed that the collapsing sheath could be represented by a collisionless Child–Langmuir (CL) sheath sandwiched between the cathode surface and the first mesh point of the adjoining numerical cell (see Fig. 3). This mesh point had previously been on the cathode surface. If the CL sheath is presumed to be one Debye length λ_D wide, then its voltage drop can be found from the incident ion flux from the gas-phase plasma model. With this approximation we have

$$V_{CL}=\left[\frac{9}{4}\left(\frac{m_i}{2e}\right)^{1/2}\frac{j_i\lambda_D^2}{\epsilon_0}\right]^{2/3}. \tag{4}$$

Here j_i is the ion current toward the wall, m_i is the ion mass, e is the unit electronic charge ($e>0$), and ϵ_0 is the permittivity of free space. The computational cells adjacent to the face of the cathode are usually $2\text{–}5\times10^{-2}$ cm wide in our model, which is comparable to the electron mean free path in a typical BLT (0.5 Torr H_2). Sheaths less than a half cell wide can therefore be considered "collisionless" and are amenable to this procedure. The approximation improves as the plasma density builds and the sheath shrinks, and therefore should be excellent during the conduction phase. Since V_{CL} is a function of ion current, which is a function of position on the cathode, the temperature and electric field at the cathode surface, and hence the cathode emission, must be calculated at each location on the surface of the cathode.

When the electric potential is obtained from solving Poisson's equation, boundary values are required on the computational mesh adjacent to the cathode. With the CL sheath, the potential on the computational mesh at these points is not equal to the cathode voltage. The boundary value for the potential on the computational mesh at location s (a function of r,z) adjacent to the cathode is then $V_b(s)=V_c+V_{CL}(s)$ where V_c (negative) is the cathode voltage obtained from the circuit equations and V_{CL} is positive. Poisson's equation is solved using the method of successive overrelaxation.

After having just completed an update to the fluid transport equations, these algorithms are implemented in the following fashion sequence: (i) The ion flux toward the cathode is determined at the center of each cell adjacent to the cathode; (ii) the Child–Langmuir voltage drop V_{CL} is calculated using the CL sheath width of one Debye length; (iii) the electric potential is obtained by solving Poisson's equation using $V_b(s)$ as the boundary value on the computational mesh; (iv) the power flux onto the cathode due is calculated to obtain the cathode surface temperature; (v) the thermionic electron current is obtained from Eq. (2).

The energetic ion impact current used to calculate the rate of cathode heating is obtained from the flux Γ of ions in the center of a cell adjacent to the cathode surface, $\Gamma=n_i\mu e-D\nabla n_i$, where μ is the ion mobility and D is the ion diffusion coefficient. The impact energy is taken to be the sum of the kinetic energy at cell center $m_iv_i^2/2$, the voltage drop from the center to edge of the computational cell, and CL sheath voltage drop V_{CL} (see Fig. 3).

To calculate the surface temperature as specified by Eq. (1), the past history of the ion flux must be known. To avoid storing an excessive amount of data points (corresponding to the location s of each mesh point on the cathode surface at each recalculation of the impinging power), the following storage method is used. The ion power flux is held in an array of points corresponding to position s and elapsed time τ. The power for the most recent time is stored as $P(s,\tau=0)$. The power for the previous two time steps is averaged and stored as $P(x,\tau=-\Delta\tau)$, which occupies a "bin" $2(\Delta\tau)$ wide. Each successively "earlier" time bin is twice as wide in time as the time bin immediately preceeding it (later in time). When a new $P(s,0)$ is calculated, the $P(s,\tau)$ array is shifted one $\Delta\tau$,

$$P[s,\tau=(-i)\Delta\tau]$$
$$=(1-1/i)P[s,\tau=(-i)\Delta\tau]$$

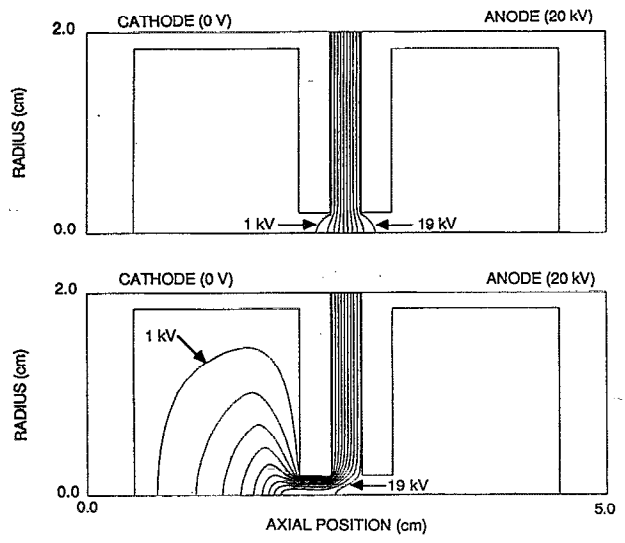

FIG. 4. Electric potential contours for (top) vacuum and (bottom) 20 ns after the start of phototriggering. The contour spacing is 2 kV. Operating parameters are an initial holdoff voltage 20 kV, gas pressure 0.5 Torr H_2, electrode separation 0.3 cm, and electrode hole radius 0.25 cm. The penetration of the anode potential into the hollow cathode extends to 18 kV.

$$+(1/i)P[s,\tau=-(i+1)\Delta\tau]. \quad (5)$$

This shifting procedure must start at $i=n$, the earliest time bin. $P(s,0)$ is then set equal to the current ion power flux. For 10-ps-wide bins at $\tau=0$, only $n=16$ time bins are required to hold the power flux history for ≈ 1 μs. This method also retains the greatest detail about the most recent power flux history, the portion which is weighted most heavily by the convolution integral in Eq. (1).

D. Status of present model

The explicit nature of the integration used here does not allow us to simulate in a fully self-consistent fashion the full voltage collapse following the onset of the "superdense glow" during the conduction portion of BLT operation in a reasonable amount of computer time. It is possible, however, to simulate BLT operation well into the formation of the hollow cathode effect [Fig. 4(b)] and the onset of the voltage collapse. Since the gap between the planar portions of the BLT electrodes is, by design, insulating, the superdense glow must be initiated before the voltage across the BLT collapses. Simulation of the BLT from trigger to the onset of voltage collapse is therefore sufficient to answer many questions about the processes responsible for eventual formation of the superdense glow conduction phase of BLT operation. Later we will make an additional approximation that allows us to simulate the entire voltage collapse. In this subsection we will discuss the results of the just-described model and show that additional physical mechanisms must be invoked to explain the extraordinarily high ion bombardment heating rate and subsequent superdense glow formation.

Previous studies[1-3] have concluded that ion bombardment is the most likely cathode heating mechanism, and that field-enhanced thermionic emission can (given sufficient field and cathode heating) explain the observed BLT conduction current densities. In the previous subsection we discussed the addition of these mechanisms to the BLT model. This model has been run for a variety of BLT geometries, charging voltages, and gas pressures. At no time does the model predict significant cathode heating, much less melting and field-enhanced thermionic emission in the experimentally observed locations. The heating rate on the face of the cathode (location A in Fig. 1) by ion bombardment from triggering to the onset of voltage collapse is perhaps five orders of magnitude smaller than that required to reproduce the experimentally observed melting.[17] Furthermore, the predicted heating rate is maximum either inside the cathode hole (location B in Fig. 1) or even inside the hollow cathode (location C in Fig. 1), and not on the front face of the cathode, where superemission is experimentally seen. Cathode erosion has been experimentally observed at all these locations, however.

We therefore conclude that additional physical mechanisms, beyond those described here, must be considered to explain the observed cathode melting and formation of the superdense glow discharge.

IV. ADDITIONAL CONSIDERATIONS FOR CATHODE HEATING

In this section we will examine the differences between experimental observations and the results of the model presented in Sec. III. We will propose additional physical mechanisms and test them by adding them to our BLT model.

A. Discharge nonuniformities

The calculation for the cathode heating rate presumes that the discharge is uniform across the cathode surface. Previous studies of BLT cathode surfaces using scanning electron microscopy have shown that the surface is not smooth on a 1–10 μm spatial scale.[1-5] The source of this roughness is believed to be many cycles of melting and freezing of the surface following current pulses. It is therefore likely that the discharge current is not microscopically uniform, but is preferentially located on microscopic surface protrusions where the electric field is enhanced. An analogous enhancement is well known in vacuum breakdown.[18] To account for this microscopic filamentation, one can assume that ion current to the cathode is collected only through a fraction of the surface f_A representing the electric-field-enhanced spots. It is difficult to calculate f_A, however, by examining scanning electron microscope images of the surface one can estimate that f_A is bounded $10^{-2}<f_A<1$. $f_A=1$ corresponds to a perfectly uniform glow, while $f_A=0.01$ corresponds to, for example, 1-μm-diam microstreamers laterally separated by 3–4 μm.

We parameterized f_A in the model and found that if microfilaments were the only effect that increases ion power flux to the degree required for melting, $f_A<10^{-5}$, which is unrealistic. Even with such an extreme assumption, the model predicts melting on the hollow side of the cathode or in the cathode hole, which does not match the

experimentally observed pattern of melting on the cathode face.[18] Furthermore, there appears to be no mechanism for the high-current plasma on the BLT axis to migrate outward in the gap and lead to formation of the superdense glow.

The aforementioned surface roughness can also lead to electric-field enhancement. The enhancement in the surface electric field at those points can also be characterized in the model by a multiplicative factor f_E. (A value of $f_E=1$ is a perfectly smooth surface; large values of f_E correspond to a rough surface with significant enhancement.) Equation (2) suggests that pure electron-field emission is insignificant for field strengths $<10^7$ V cm^{-1}. This high value for the onset of emission is experimentally seen only for carefully prepared metallic micropoints.[16,19,20] The electric field at the onset of emission for broad area electrodes nominally occurs at $\sim 10^5$ V cm^{-1},[19,20] corresponding to $f_E = 10^2$ for our conditions, and may occur at much lower field strengths, corresponding to $f_E \approx 2000$. Such enormous field enhancements are usually not entirely due to surface roughness but are apparent enhancements to the metal's emission characteristics due to surface oxides, hydrocarbons, and dielectric dust. These latter conditions do not apply to a well-conditioned BLT cathode surface. Although oxides and hydrocarbon films should not be found in an operating BLT, an adsorbed layer of H should exist during holdoff as long as the device is near room temperature. This effect will be discussed below. In this work we considered field-enhancement factors which correspond to clean metallic surfaces, $1 < f_E < 10^2$. When these values are used in the model, we fail to observe the onset of thermal emission.

An electric field at the cathode surface enhanced by $f_E \lesssim 10^2$ is again insufficient to explain the observed cathode emission. It does, however, lead to some intriguing new physical mechanisms in the gap region of the BLT. The macroscopic field in a 0.2 cm gap for a 50 kV holdoff potential is 2.5×10^5 V cm^{-1}. This electric field may cause electron emission, though the field is still a factor of ≈ 4 less than the fields nominally associated with vacuum breakdown experiments.[18] The magnitude of this field emission current can be estimated from the measured "off" state current of the BLT, which is no greater than μA–mA. This is consistent with the field emission current found from Eq. (2) by using reasonable field-enhancement factors $f_E < 10^2$.

The cold cathode field emission pattern is strikingly similar to the ultimate melting pattern; that is, the highest fields during the holdoff phase are on the face of the cathode near the cathode hole. However, there does not appear to be any method for this field to, by itself, initiate the superdense glow. Electrons that are field emitted during holdoff stream nearly collisionlessly across the gap since, by definition, the electrode configuration is insulating, at least for pulse charging. The electrons impinge on the anode surface and can release adsorbed H with perhaps unit efficiency and producing H^+ with an efficiency of ≈ 0.01.[19,20] They also likely result in a small amount of gas-phase ionization. For typical dark currents, however, the H and H^+ desorption produce only a negligible increase in the neutral density and BLT current, respectively. Nonetheless, this field emission and subsequent desorption and ionization probably preionizes the gap region. Presuming a dark current of 1 mA cm^{-2} and that 0.01 H^+ ions are desorbed for every incident ion, the plasma density in the gap during holdoff (20–200 kV cm^{-1}) is small, on the order of 10^5–10^6 cm^{-3}. Again, when using this value of preionization for the gap in the model, we fail to observe the onset of thermal emission.

B. Photon-induced processes

We have to this point examined only plasma and neutral particle production and transport mechanisms to initiate the observed superdense glow. These mechanisms have failed both quantitatively (not enough heating) and qualitatively (not heating the cathode face) to explain the initiation of the superdense glow. The primary failure has been to produce an insufficient density of plasma between the electrode faces at radii larger than the electrode holes. Field emission from the cathode face produces insufficient gap ionization, and the high density of plasma ions on the longitudinal axis of a switching BLT cannot diffuse radially during the short time scale of BLT operation.

Recall that the three stages of commutation in the BLT proceed from conventional hollow cathode emission, to a stage in which there is high current on the axis, and finally to a superdense glow on the cathode surface. Visual and spectroscopic observations have been made of the optical emission from the on axis current to measure electron densities and to chart the stages of commutation.[1–3] The light emission during the second stage is intense and given sufficient photon energy, such photons also can desorb surface species, and excite and ionize gas-phase species. Photo-induced ionization of gas-phase molecules in the otherwise insulating gap in some sense represents an external source of ionization, and as such can make the gap conducting. The time scale for these effects is essentially instantaneous compared to the electron or ion transit time (one to tens of ns), or the ion diffusion time (μs–ms). We believe that photon-induced processes in the gap, and ionization in particular, resulting from UV emission originating from the on-axis current during commutation is largely responsible for the onset of the superdense glow.

We have previously determined that the photoproduction of electrons on the inside of the hollow cathode has a negligible effect on the electron photoemission on the back side of the cathode.[9,17] We have therefore included in this study only the photoionizations resulting from photon production in the electrode holes and the electrode gap. To examine these effects, we will parameterize the production of UV photons as being proportional to the rate of electron-impact ionization of ground state H_2 (the "primary ionization rate"). This function is expressed as a photon generation efficiency η. During commutation both the charged particle density and the primary ionization rate are maximum along the BLT axis, and the η photons eventually resulting from these ionizations are presumed to radiate isotropically from the location of the primary ion-

ization. Photoionization in the gap, either directly or by a multistep process, is included in the model by calculating the ground-state ionization rate in the gap and multiplying by η to obtain a spatially dependent rate of production of radiation. Using this source function, we perform a photon transport calculation to obtain the ionization rate in the gap, while accounting for the particulars of electrode shadowing and divergence in the cylindrical geometry. We note that because of the r^{-2} dependence in the radiating photon flux the highest photoionized particle density in the gap will always be near the BLT axis. The area of the cathode face nearest the cathode hole will therefore always receive the highest ion power flux, and emission from this area will "switch on" before areas farther from the BLT axis.

Although we may speculate as to the exact photon-induced ionization mechanism, a thorough study of the precise mechanism is beyond the scope of the present work. Photons in the gap are produced by a variety of gas mechanisms (recombination, direct electron impact, cascade processes) as well particle impact on metal surfaces. The photoionization cross section we used here for ground state H_2 is $\approx 1\times10^{-17}$ cm^2 at 750 Å.[21] Although the amount of radiation at this wavelength is most likely small, the photoionization process can proceed fairly rapidly through a variety of multistep processes. Our goal here is only to demonstrate that, given reasonable assumptions for the ultimate photoionization yield, our model predicts significant heating of the cathode surface in the experimentally observed pattern, and that the postulated mechanism can initiate the conduction phase superdense glow discharge. We will explore specific photoinduced mechanisms in future work.

We now summarize the sequence of events of our photo-induced cathode emission model: (i) Photons produced by electron-impact processes on the axis of the BLT gap radiate instantaneously into the gap region outside the electrode holes, leading to gas phase photoionization; (ii) the FNBS equation predicts greater electron emission at intermediate temperatures and surface field strengths (where the BLT tends to operate) than one would expect from a simple sum of pure thermal and pure field emission; (iii) field-enhanced thermionic emission, coupled with moderate photoionization of the gap, leads to the observed pattern of electron emission and cathode erosion.

V. RESULTS FROM BLT MODEL WITH PHOTO-INDUCED EFFECTS

We now present results from the BLT model including photo-induced effects. In the cases presented below the "beam-bulk" option of the model is not used. We found that found that the $I(t)$ behavior is adequately represented by the drift-diffusion electron model with momentum and energy accounting even during the switching phase when the greatest nonequilibrium electron effects are expected.

In our parametrizations, we found that having a constant photogeneration efficiency (as a function of time) from the beginning of commutation leads to premature gap breakdown, a consequence of there being an external source of ionization. We found that premature gap breakdown will occur if η is nonzero for currents $\lesssim 10^{-3}$ A. Since the ultimate rate of photoionization depends on multistep processes, it is reasonable to expect that η should increase with increasing current. We also found that as long as premature breakdown does not occur, the model predictions are relatively insensitive to the details of the dependence of η on current. We have therefore chosen to linearly increase η as a function of current to its final value at 1 A.

A. Distribution of cathode heating

Voltage contours both at triggering and 20 ns after triggering are shown in Fig. 4 for our baseline BLT conditions: 20 kV holdoff, 0.3 cm electrode gap, 0.2 cm electrode hole radius, and 0.5 Torr H_2. We note here that the precise anode delay time is dependent upon the magnitude of the triggering photon flux[9] and as such is somewhat arbitrary. We chose a sufficiently large initiating photon flux so that the anode delay time is only a few tens of ns. The results are otherwise insensitive to the anode delay time. The holdoff condition [Fig. 4(a)] shows the expected voltage contours for the electrode geometry and holdoff voltage in the absence of a plasma. At $t=20$ ns, the hollow cathode effect is evident, as more than 90% of the anode potential has penetrated through the cathode hole. Since significant heating of the cathode has not yet occurred, this result, along with predictions for other plasma parameters such as density and ionization rate, are similar to those presented in a previous study.[7]

The cathode heating power at $t=20$ ns for the same BLT conditions is shown in Fig. 5(a) for photon generation efficiencies $0<\eta<10$. For $\eta\geq 3$, the highest power flux is found near the cathode hole. As η is increased, the maximum heating rate migrates from the inside the hollow cathode (location C in Fig. 1) to the face of the cathode (location A in Fig. 1). The time evolution of the distribution of heating power for the baseline conditions is shown in Fig. 5(b). Note that, as a function of time, the power flux increases logarithmically at all locations during this phase of BLT operation, while the power is preferentially enhanced on the face of the cathode as one increases η.

B. Cathode heating dependence on BLT conditions

The results of a survey of the cathode heating rate as a function of BLT parameters are shown in Fig. 6. We have fixed the photogeneration efficiency to be $\eta=3$ in all cases, and have run the BLT model to a prespecified current, typically 10 A. As discussed in the previous section, the peak ion heating power and the BLT current obey a power-law relationship versus time once initial transients are over and before significant voltage collapse occurs. This allows us to run the BLT model to a prespecified current and compare cathode heating rates for various choices of fill gas pressure, electrode gap, cathode hole radius, and holdoff voltage. The results in Fig. 6 therefore represent relative heating rates during the switching phase as a function of initial BLT conditions, and as such gives some indication as to how one might adjust operating conditions to alter cathode heating and emission.

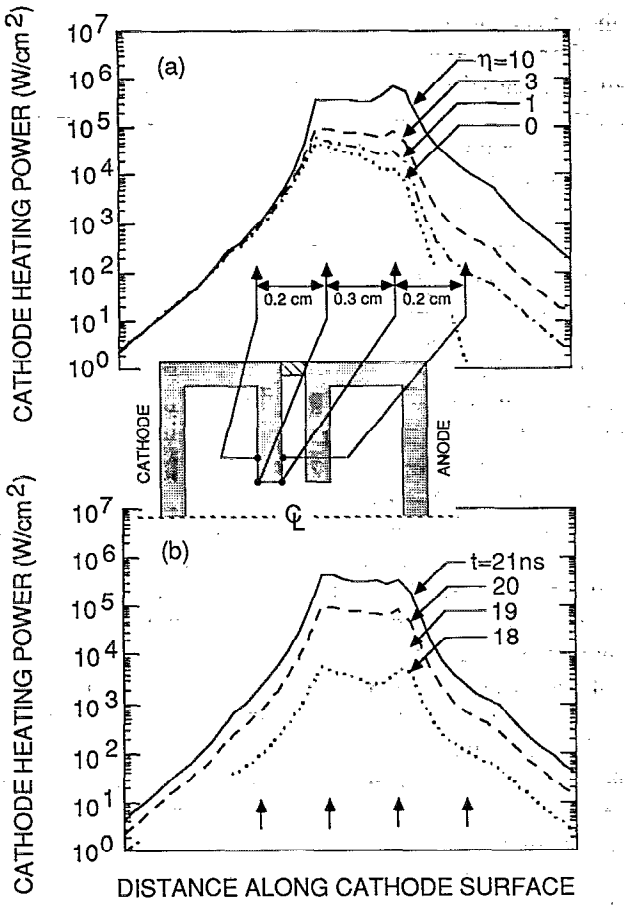

FIG. 5. Cathode heating power as a function of location on the cathode surface. The inset relates points on the plot to locations on the cathode surface. (a) Cathode heating as a function of increasing effective photogeneration yield η. Increasing η not only increases the heating power, but changes the location of maximum heating from the cathode hole wall to the front face of the cathode. (b) Time evolution of the heating power for $\eta=3$. Note that location of maximum heating power does not change.

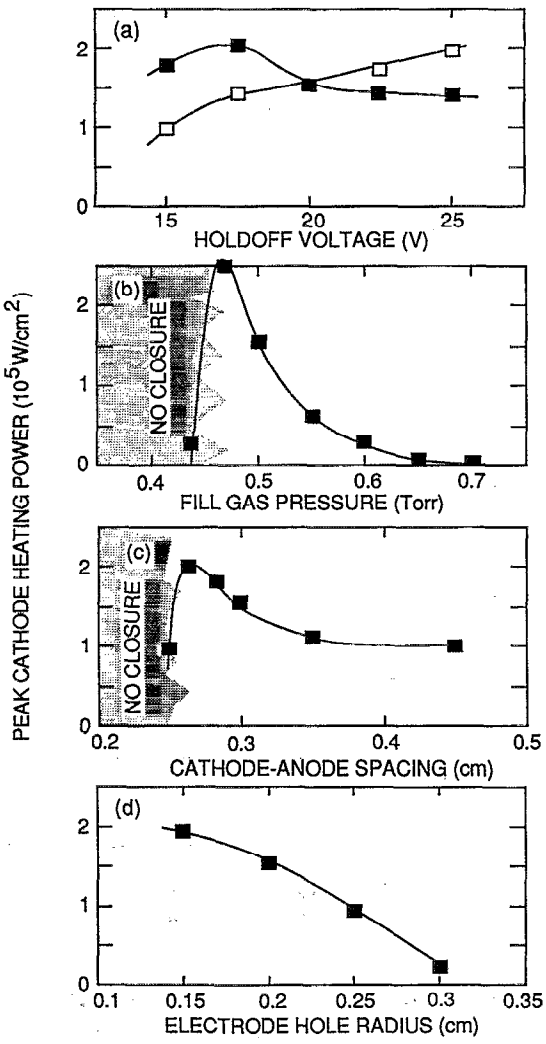

FIG. 6. Maximum heating power on the surface of the cathode as a function of various BLT switching parameters. The baseline conditions are an initial holdoff potential of 20 kV, 0.5 Torr H_2, 0.3 cm electrode spacing, and 0.25 cm electrode hole radius. Each of these parameters is then varied: (a) initial holdoff potential; (b) fill gas pressure; (c) electrode spacing; and (d) electrode hole radius. Heating power increases as the operating point is moved closer to the point at which the BLT will no longer close (lower values of *pd* or smaller cathode hole diameters).

The peak cathode heating rate as a function of initial holdoff voltage is shown in Fig. 6(a). The heating rate is plotted at two different currents. The first is at a fixed value of 10 A. The second heating rate is at a current normalized by the initial holdoff voltage: 7.5 A for 15 kV, 10 A for 20 kV, 12.5 A for 25 kV, and so on. This roughly corresponds to plotting the heating rate at the same fractional voltage drop. We find that the heating rate increases with holdoff voltage for a fixed voltage drop, but decreases with holdoff voltage for a fixed BLT current. This trend results from the fact that as the holdoff voltage increases, increases in current are equally obtained by higher drift velocities as higher plasma density. Since electron-impact rate coefficients are weak functions of voltage over this range, there is less production of ionizing radiation.

The effects of fill gas pressure and electrode spacing on cathode heating are shown in Figs. 6(b) and 6(c), respectively. The heating rate increases as one decreases either the pressure or gap spacing (or their product) until one approaches the pressure-gap product below which the BLT will no longer switch. At this point, the heating rate drops. Similarly, the cathode heating is found to increase as the electrode hole radius is decreased [see Fig. 6(d)], which also corresponds to a higher holdoff voltage.[9] We therefore conclude that the initial cathode heating rate is maximum if one operates at the minimum pressure-gap product and hole radius for which the BLT will close when triggered.

C. Cathode surface melting during conduction

With some modifications (discussed in the Appendix), the BLT model can simulate the onset of thermionic emission and the superemissive conduction phase. The predicted cathode temperature distribution is shown in Fig. 7 at a current of 182 A. The conditions are the same as in Figs. 3 and 5(b). At 182 A, a portion of the cathode surface is molten, both inside the cathode hole and extending along the face of the cathode. A second hot spot on the cathode surface (which itself melts later in the calculation)

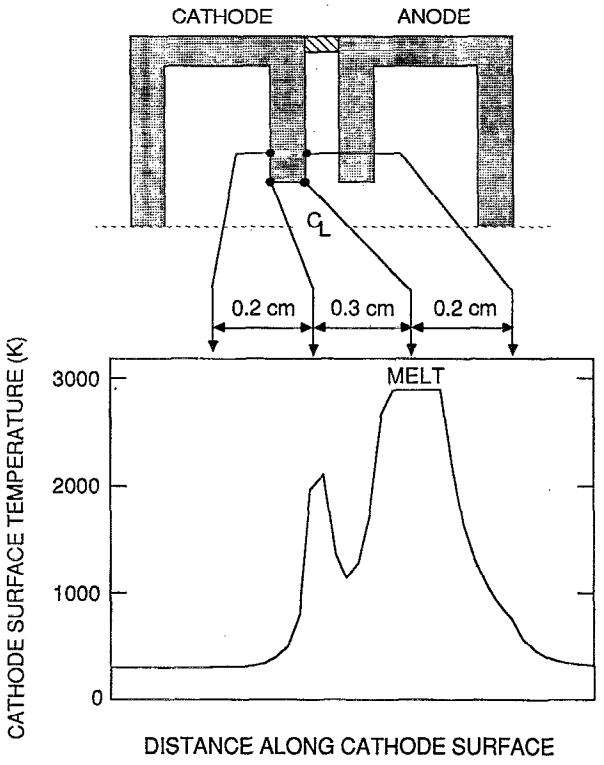

FIG. 7. The cathode surface temperature at a BLT current of 182 A. The conditions are the same as in Figs. 4 and 5(b). The inset relates points on the plot to locations on the cathode surface. Melting occurs on the face of the cathode and at the vertex of the cathode hole.

is at the edge of the cathode hole nearest the hollow cathode. We have based our cathode heating calculation on an investigation into cathode heating mechanisms by Hartmann *et al.*[1] In that work, a cathode heating power of 10 MW cm^{-2} for 100 ns duration was assumed for illustration purposes. We found that it was difficult to sustain this rate of heating for as long as 100 ns. Although the mechanisms ultimately responsible for the onset of thermionic emission are very similar to those discussed by Hartmann *et al.*[1] the actual rate of heating that we calculate is different. We find that the cathode heating power peaks at 10^8–10^9 W/cm^2 over a narrow annulus (<1 mm wide) surrounding the cathode hole for <10 ns. A similar amount of energy is delivered to the cathode surface over a shorter period of time. The onset of thermionic emission so predicted is therefore more abrupt.

VI. SUMMARY AND CONCLUDING REMARKS

At triggering, the electric field in the gap is sufficient to cause some field emission of electrons from the cathode given reasonable assumptions about the electric-field enhancement on a conditioned broad area electrode. It is therefore likely that the BLT gap is preionized to a relatively low plasma density ($<10^6$ cm^{-3}) by field-emitted electrons. However, the gap is, by design, insulating, and this moderate plasma density can neither trigger the BLT, nor initiate the large area cathode surface heating and emission that is experimentally seen. After triggering, the photoelectrons from the inner surface of the cathode are accelerated in the vacuum fields and avalanche, leading to an exponential increases in the density and ionization rate on the BLT axis near the electrode gap. Photons generated by electron-impact excitation, recombination, and cascade processes on the BLT axis isotropically radiate into the gap region, photoexciting and photoionizing the fill gas. These photo-induced ionizations greatly increase (on a relative basis) the plasma density in the gap on a time scale that is practically instantaneous compared with the time for ion transport. The ions produced in the gap are then accelerated into the cathode by the strong gap field, heating an annulus on the face of the cathode outside the cathode hole. Many more ions are produced on the axis of the BLT (primarily through electron-impact ionization). These ions are accelerated into the cathode hole and strike the cathode on the inside of the hollow cathode electrode. However, the electric field at these locations is weak compared to that in the gap which accelerates the photo-produced ions, thereby resulting in a lower heating rate. The gap field also leads to significant field emission of electrons at moderate cathode temperatures (less than melting). The combination of a relatively low density of photo-produced ions in the gap, higher ion-impact energies in the gap, and the very strong fields at the cathode surface lead in our model to the observed broad area of melted cathode surface and high electron emission.

Given the combination of a hot or molten cathode surface, electric-field strength at the surface (even in the vacuum configuration) of $>5\times10^5$ V cm^{-1}, and reasonable estimates of the broad area surface field enhancement ($f_E<10^2$), the Fowler–Nordheim–Bethe–Sommerfeld equation predicts electron emission densities of 10^4–10^6 A cm^{-2}, which is sufficient to account for the observed BLT current. When these processes are incorporated into the model, both the pattern of the observed melting of an annulus of the cathode face around the cathode hole, and the pattern of field-enhanced thermionic emission, are reproduced.

A complete investigation of the possible photo-induced ionization mechanisms was not with the scope of the present work. We therefore chose to parameterize the effect in the most general terms possible (photon mean free path, photogeneration efficiency, and threshold current). A proper model of any photo-induced effects must necessarily include a detailed treatment of the H_2 and H electronic energy levels, cascade processes, and radiation trapping. Here we have simply demonstrated that, given some reasonable assumptions about a photo-induced ionization mechanism, one can predict the observed BLT conduction phase heating and emission patterns.

ACKNOWLEDGMENTS

The authors would like to thank John Waymouth for his comments on electric-field-enhanced thermionic emission. This work was supported by SDIO/IST managed by the Office of Naval Research (N00014-90-J-1967) and the National Science Foundation (ECS91-09326 and CTS91-13215).

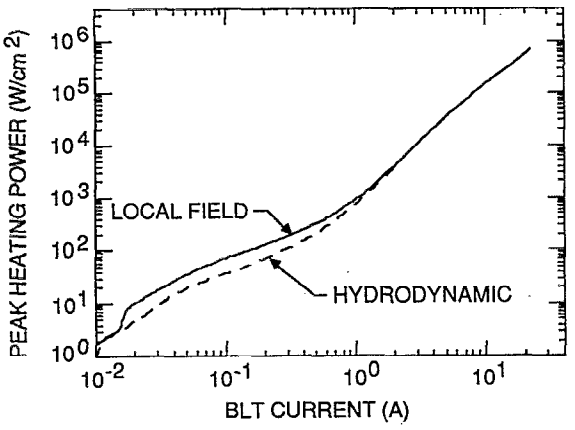

FIG. 8. Comparison of the cathode heating rate vs BLT current obtained using the local-field approximation (electron and ion continuity equations only) and the hydrodynamic BLT model (also including the electron momentum and energy equations). Once the current has exceeded ≈ 5 A, the local-field model is a good approximation to the more sophisticated hydrodynamic model.

APPENDIX: SCALING IN THE BLT MODEL

The modification required to simulate the onset of conduction in a reasonable amount of computer time is to limit the charge density that appears in Poisson's equation. This removes the strong feedback between the charged particle continuity equations and allows time steps well in excess of the dielectric relaxation time τ_{DR}. The penalty for making this approximation is that the maximum field gradient is artificially constrained, and the hollow cathode effect is not fully resolved. We refer to this model as the semi-self-consistent (SSC) BLT model.

The details of the formation of the hollow cathode do not greatly influence the heating rate of the cathode face for BLT currents below ≈ 1 A. The power-current (P-I) characteristic for the SSC model is therefore similar to that presented in Fig. 8 for the fully self-consistent model (FSC); that is, $P \sim I$. The SSC model does not predict the change in slope ($P \sim I^{2.5}$) shown in Fig. 8 for currents above ≈ 1 A, and therefore underestimates the peak cathode heating rate relative to the FSC model as the BLT evolves toward the conduction phase. We have therefore scaled the cathode heating power in the SSC model to match the predicted power-current relationship of the FSC model.

We conjectured earlier that the local-field approximation (LFA) used in the gas-phase plasma model, found in previous work to accurately predict the BLT current rise $I(t)$, should be an even better approximation as the plasma density increases. The peak heating rates as predicted by the LFA model and the hydrodynamic model are shown in Fig. 8, and indicates that, except for moderate disagreement for BLT currents < 1 A, the simplified LFA model is in excellent agreement with the more sophisticated (and computationally more intensive) hydrodynamic model.

[1] W. Hartmann, V. Dominic, G. F. Kirkman, and M. A. Gundersen, J. Appl. Phys. **65**, 4388 (1989).
[2] W. Hartmann, V. Dominic, G. F. Kirkman, and M. A. Gundersen, Appl. Phys. Lett. **53**, 1699 (1988).
[3] H. R. Bauer, G. Kirkman, and M. A. Gundersen, IEEE Trans. Plasma Sci. **PS-18**, 237 (1990).
[4] A collection of papers describing pseudosparks can be found in M. A. Gundersen and G. Schaefer, *Physics and Applications of Pseudosparks*, NATO ASI Series B: Physics, Vol. 219 (Plenum, New York, 1990).
[5] W. Benker, J. Christiansen, K. Frank, H. Gundel, W. Hartmann, T. Redel, and M. Stetter, IEEE Trans. Plasma Sci. **PS-17**, 754 (1989).
[6] G. Kirkman-Amemiya, N. Reinhardt, M. S. Choi, and M. A. Gundersen, in *Digest of Technical Papers of the Eighth IEEE International Pulsed Power Conference*, edited by K. Prestwich and R. White (IEEE, New York, 1991), pp. 482–485.
[7] Hoyoung Pak and M. J. Kushner, Appl. Phys. Lett. **57**, 1619 (1990).
[8] J.-P. Boeuf and L. C. Pitchford, IEEE Trans. Plasma Sci. **PS-19**, 286 (1991).
[9] Hoyoung Pak and M. J. Kushner, J. Appl. Phys. **66**, 2325 (1989).
[10] H. Pak, Ph.D. thesis, University of Illinois, 1991.
[11] K. Mittag, P. Choi, and Y. Kaufman, Nucl. Instrum. Methods. Phys. Res. A **292**, 465 (1990).
[12] M. S. Barnes, T. J. Colter, and M. E. Elta, J. Appl. Phys. **61**, 81 (1987).
[13] Y. S. Touloukian, in *A Physicist's Desk Reference*, edited by H. L. Anderson (AIP, New York, 1989), p. 336.
[14] R. W. Weast, *Handbook of Chemistry and Physics*, 49th ed. (Chemical Rubber Co., Cleveland, OH, 1968).
[15] F. A. Maxfield and R. R. Benedict, *Theory of Gaseous Conduction and Electronics* (McGraw-Hill, New York, 1941), p. 148.
[16] W. P. Dyke and W. W. Dolan, in *Advances in Electronics and Electron Physics*, edited by L. Marton (Academic, New York, 1956), p. 89.
[17] T. J. Sommerer, H. Pak, and M. J. Kushner, in 44th Annual Gaseous Electronics Conference, Albuquerque, NM, 1991, paper PC-7.
[18] F. R. Schwirzke, IEEE Trans. Plasma Sci. **19**, 690 (1991).
[19] J. Halbritter, IEEE Trans. Electr. Insul. **EI-18**, 253 (1983).
[20] J. Halbritter, IEEE Trans. Electr. Insul. **EI-20**, 671 (1985).
[21] L. C. Lee, R. W. Carlson, and D. L. Judge, J. Quant. Spectrosc. Radiat. Transfer **16**, 873 (1976).